Supporting Information

Efficient One-Step SO_2 Capture from Industrial Flue Gas via a Scalable Zr-Based Metal-Organic Framework

Si-Chao Liu[a], Li Xu[a], Li-Ping Zhang[a], Chen-Xu Li[b], You-Xiang Lu[b]*, Yi-Tao Li[a], Jian Wang [b]*, Shao-Min Wang[a]*, Qing-Yuan Yang[a]*

[a]State Key Laboratory of Fluorine & Nitrogen Chemicals, School of Chemical Engineering and Technology, Xi'an Jiaotong University, Xi'an, Shaanxi 710049

[b]Anhui Provincial Key Laboratory of Aerosol Analysis, Modulation and Biological Effect/China Tobacco Anhui Industrial Co., Ltd.

E-mail: 574567981@qq.com; wangj86@mail.ustc.edu.cn; shaominwang@xjtu.edu.cn; qingyuan.yang@xjtu.edu.cn

1. Supplemental Experiment Procedures

Breakthrough experiments:

The breakthrough experiments were conducted on a dynamic gas breakthrough setup. The sample packaging material is a U-shaped glass tube with an inner size of φ = 4 × 160 mm, and quartz cotton is filled at both ends. Then the samples in U-shaped glass tube were activated by helium flow at 150℃ (30 mL/min) for at least 2 h. The flow rate of the mixed gas is controlled by a mass flow controller (MFC). Outlet gas from the column was continuously monitored using gas chromatography (GC 9790 II) equipped with a thermal conductivity detector (TCD). The n-butane and iso-butane gas flows were both controlled at 0.2 mL/min. In cyclic breakthrough experiments, the sample regenerated by purged with helium gas at 30 mL/min for 3 h at 120℃ between each breakthrough. The gas adsorption capacity in column can be determined by Eqn (1):

$$q_i = \frac{v \times V\%}{22.4} \times \int_{t_1}^{t_2} (c_0 - c_i)dt = \frac{v \times V\%}{22.4} \times S \quad (1)$$

In equation (1), q_i (mmol/g) is the adsorption capacity of component i, v is the flow rate of the gas mixture, $V\%$ is the molar fraction of SO_2, CO_2, or N_2. c_0 and c_i are the outlet and inlet fraction of gas component i, respectively.

Calculation of isosteric enthalpy of adsorption (Q_{st}):

The Q_{st} for SO_2 and CO_2 were fitted by the virial equation (Eqn (2)) according to the isotherms at different temperatures. The fitting parameters were then used to calculate the Q_{st} using Eqn (3) [1].

$$y = \ln(x) + \frac{1}{T}\left(a_0 + a_1x + a_2x^2 + a_3x^3 + a_4x^4 + a_5x^5\right) + \left(b_0 + b_1x + b_2x^2 + b_3x^3\right) \quad (2)$$

$$Q_{st} = -8.314 \times \left(a_0 + a_1q + a_2q^2 + a_3q^3 + a_4q^4 + a_5q^5\right) \quad (3)$$

Where a_i and b_i are virial coefficients required to describe the isotherms in detail. q represents the adsorption capacity (mmol/g) at different times at a constant temperature.

Calculation of selectivity via IAST:

Single-component gas equilibrium adsorption isotherms were fitted with the dual-site Langmuir-Freundlich model, given by the following equation:

$$y = \frac{a1 \times b1 \times x^{c1}}{1 + b1 \times x^{c1}} + \frac{a2 \times b2 \times x^{c2}}{1 + b2 \times x^{c2}} \quad (5)$$

Where y is the gas adsorption capacity (mmol/g), a is the saturated adsorption capacity of the gas (mmol/g), and b is the Langmuir parameter in kPa^{-1}, x is the gas pressure in kPa, c is the dimensionless Freundlich parameter, and subscripts 1 and 2 correspond to two different identities. The fitting parameters of the Langmuir-Freundlich model were determined using a least-squares.

The adsorption selectivity of the binary mixture was predicted by using the Ideal Adsorption Solution Theory (IAST) [2]. The adsorption selectivity can be determined by Eqn (6):

$$S_{ads} = \frac{X_1/X_2}{Y_1/Y_2} \quad (6)$$

Where S is the selectivity of component 1 relative to 2. X_1 and X_2 are the molar fractions of components A and B in the adsorption phase, respectively. Y_A and Y_B are molar fractions of components A and B in the gas phase, respectively.

Computational details:

DFT calculations were carried out using Material Studio package. For the Grand canonical Monte Carlo (GCMC) simulations[3], the guest molecules SO_2, CO_2 and N_2

were geometrically optimized using Forcite code[4] and the electrostatic potential (ESP) charges were applied to the guest molecules. The crystal structure of the MOF-801(Zr) was optimized with Forcite code, and the optimization results matched well with the crystal structures. The gas molecules and MOF skeleton were both treated as rigid bodies. The gas-framework interactions were described by the standard universal force field (UFF) [5]. The density distribution of SO_2, CO_2 and N_2 were calculated by using the fix pressure task in Sorption module and Metropolis method. For each state point, the system was equilibrated for 1×10^6 steps, and then the ultimate data were collected for another 1×10^7 steps. The locate task simulated the beneficial adsorption sites with a single guest molecule. All CIF files were processed to remove solvents and guest molecules before computation.

Supplemental Figures and Tables

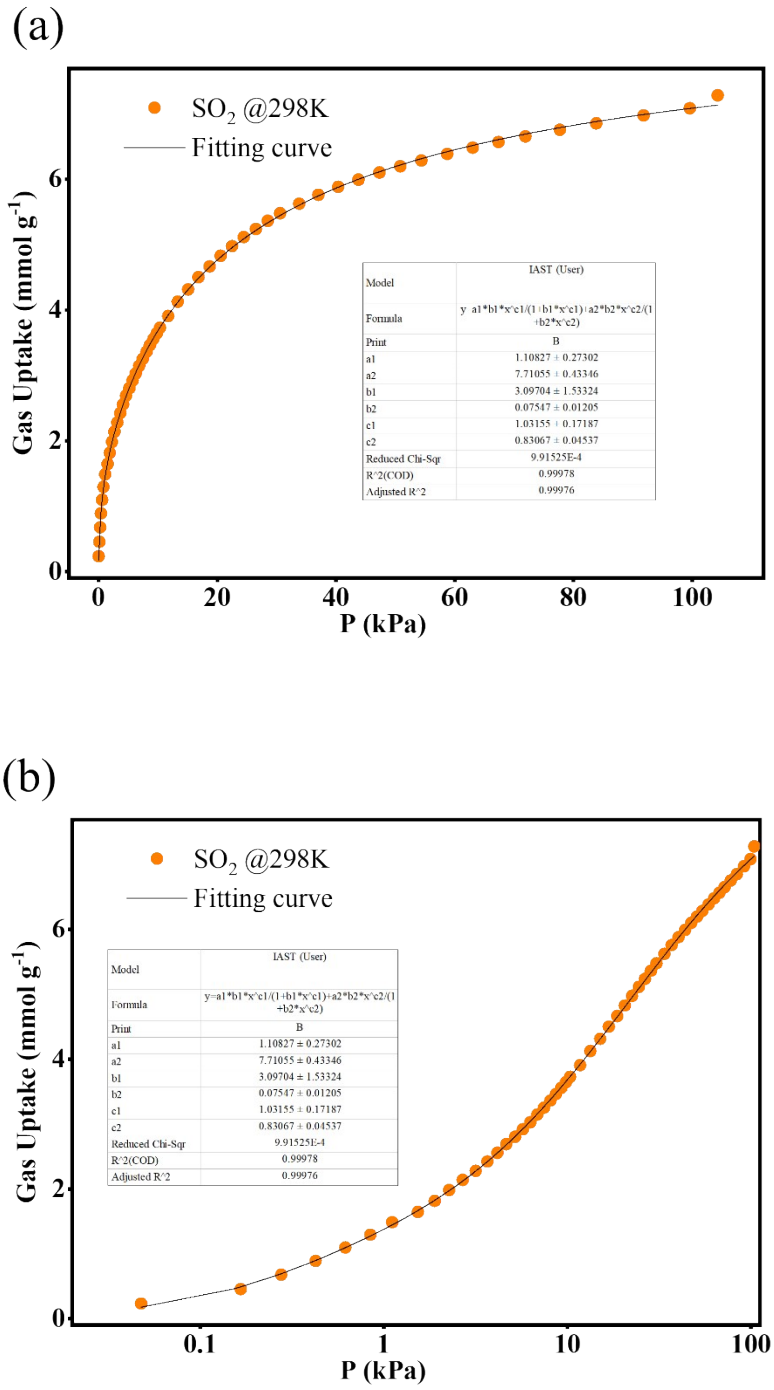

Figure S1. Dual-site Langmuir-Freundlich model for SO_2 adsorption isotherm on MOF-801(Zr) at 298 K.(a) Linear-scale plot (b) Log plot.

(a)

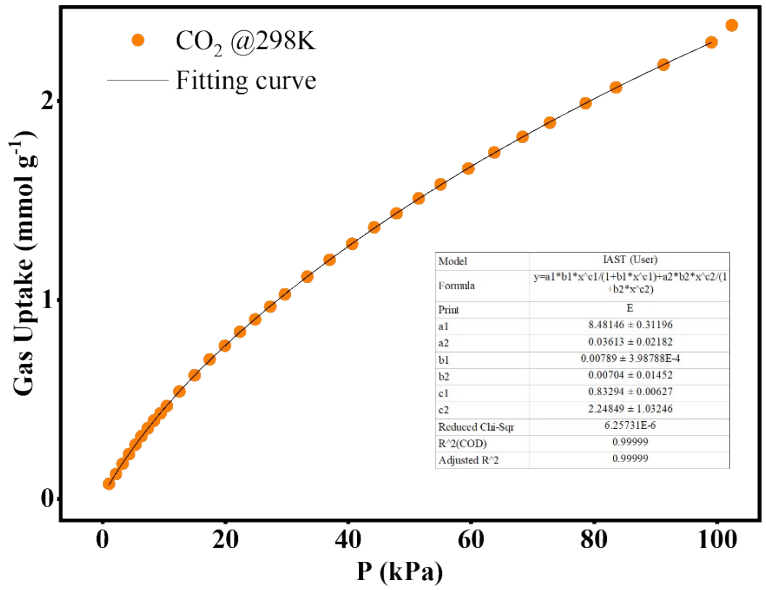

(b)

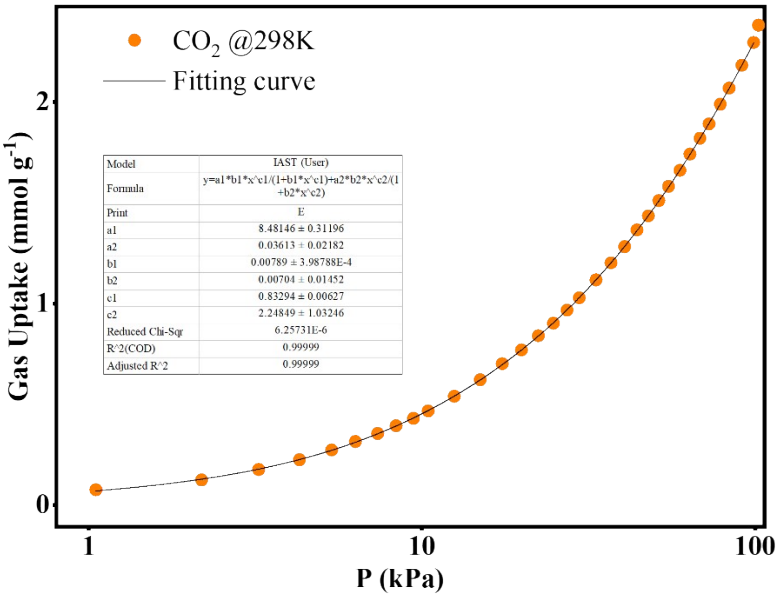

Figure S2. Dual-site Langmuir-Freundlich model for CO_2 adsorption isotherm on MOF-801(Zr) at 298 K. (a) Linear-scale plot (b) Log plot.

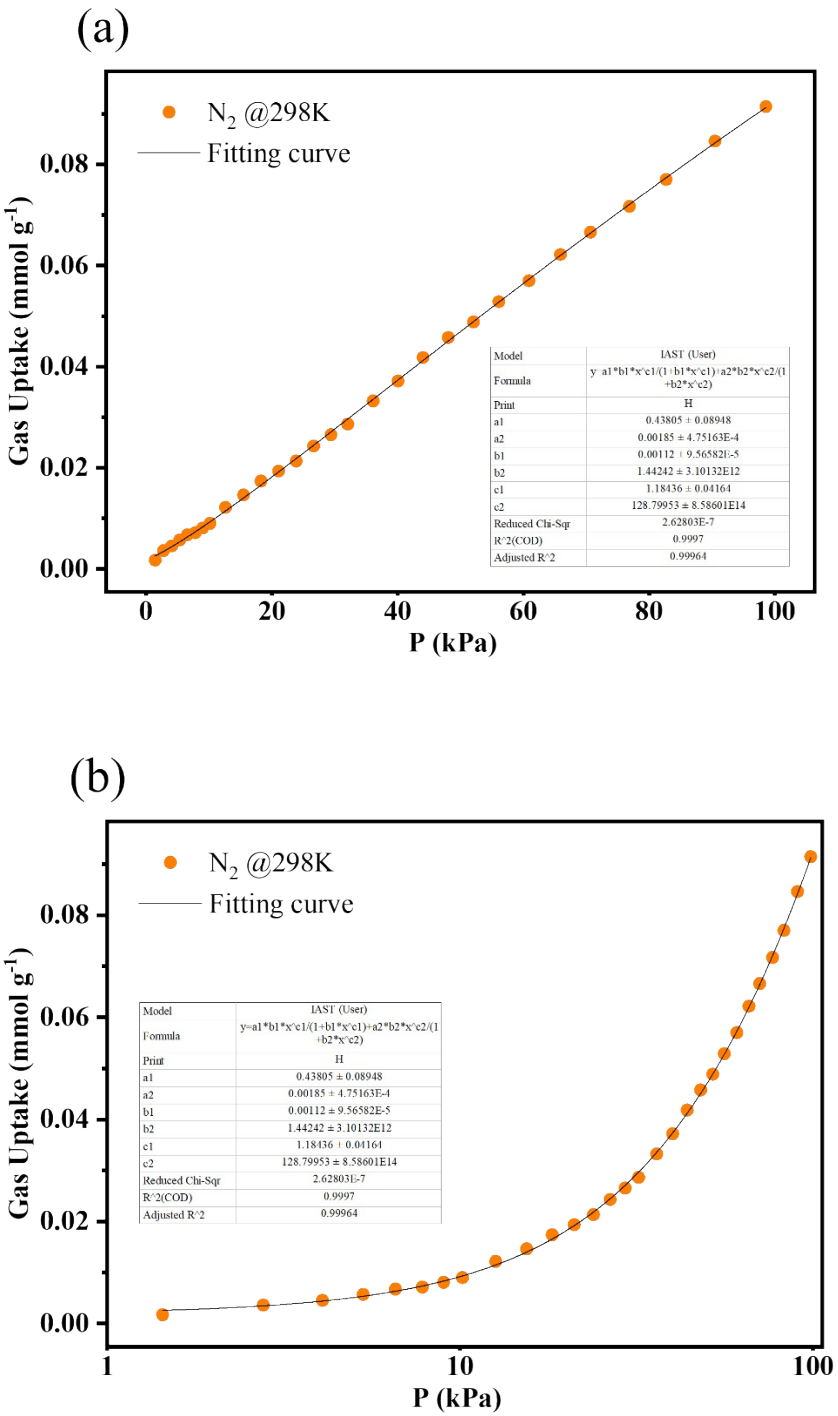

Figure S3. Dual-site Langmuir-Freundlich model for N_2 adsorption isotherm on MOF-801(Zr) at 298 K. (a) Linear-scale plot (b) Log plot.

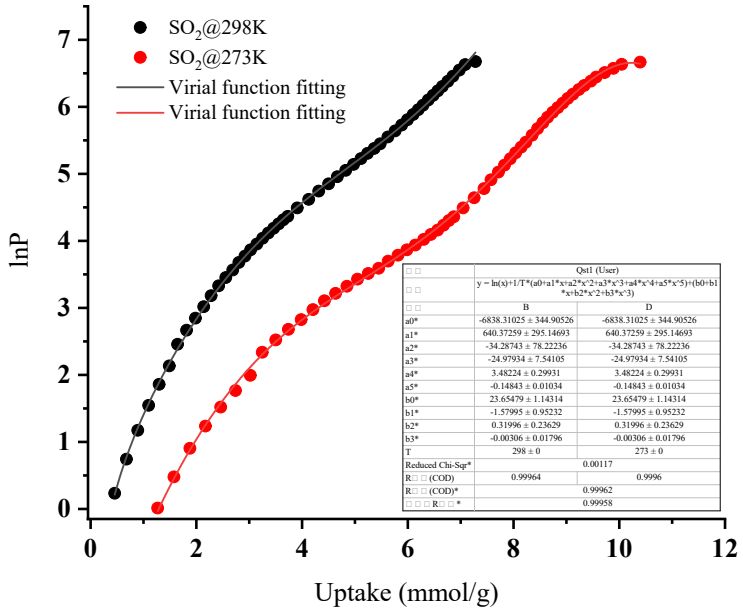

	Qst1 (User)	
	y = ln(x)+1/T*(a0+a1*x+a2*x^2+a3*x^3+a4*x^4+a5*x^5)+(b0+b1*x+b2*x^2+b3*x^3)	
	B	D
a0*	-6838.31025 ± 344.90526	-6838.31025 ± 344.90526
a1*	640.37259 ± 295.14693	640.37259 ± 295.14693
a2*	-34.28743 ± 78.22236	-34.28743 ± 78.22236
a3*	-24.97934 ± 7.54105	-24.97934 ± 7.54105
a4*	3.48224 ± 0.29931	3.48224 ± 0.29931
a5*	-0.14843 ± 0.01034	-0.14843 ± 0.01034
b0*	23.65479 ± 1.14314	23.65479 ± 1.14314
b1*	-1.57995 ± 0.95232	-1.57995 ± 0.95232
b2*	0.31996 ± 0.23629	0.31996 ± 0.23629
b3*	-0.00306 ± 0.01796	-0.00306 ± 0.01796
T	298 ± 0	273 ± 0
Reduced Chi-Sqr*	0.00117	
R□ □ (COD)	0.99964	0.9996
R□ □ (COD)*	0.99962	
□ □ □ R□ □ *	0.99958	

Figure S4. Virial fits for SO_2 on different temperature adsorption isotherms of MOF-801(Zr).

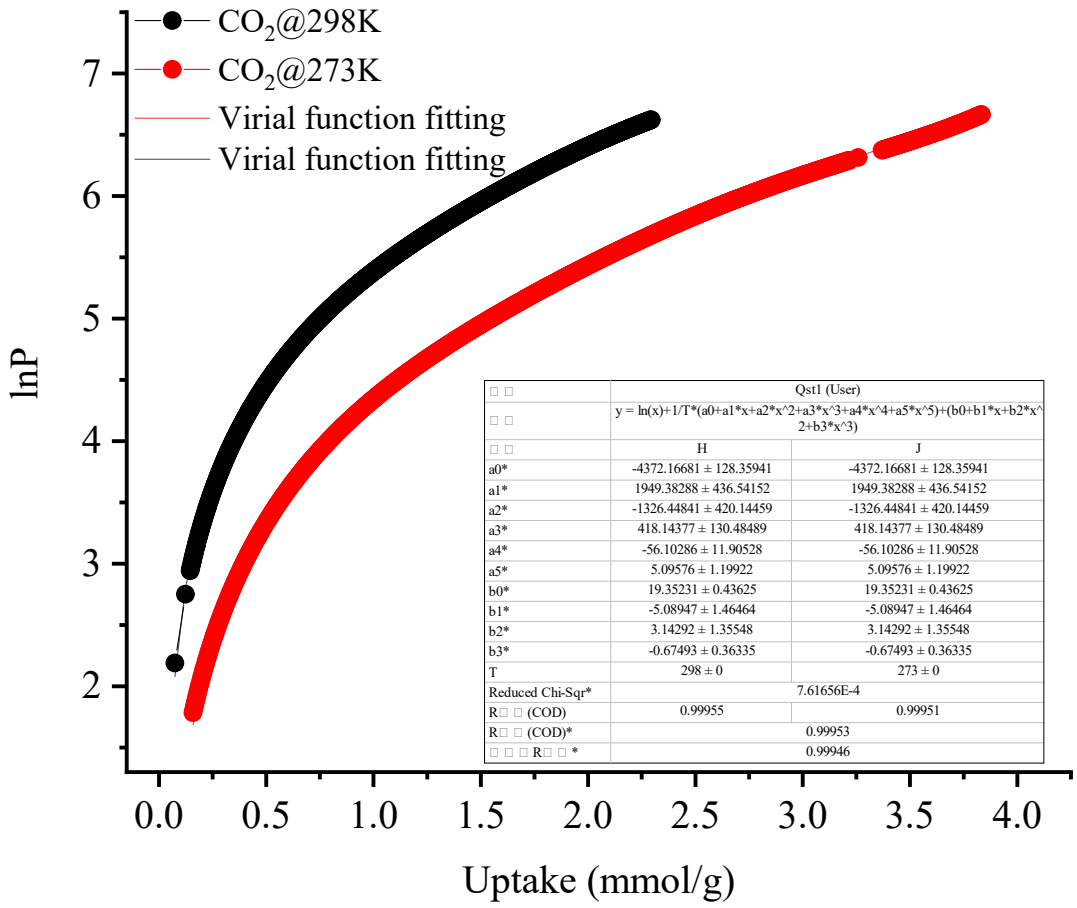

□ □	Qst1 (User)	
□ □	y = ln(x)+1/T*(a0+a1*x+a2*x^2+a3*x^3+a4*x^4+a5*x^5)+(b0+b1*x+b2*x^2+b3*x^3)	
□ □	H	J
a0*	-4372.16681 ± 128.35941	-4372.16681 ± 128.35941
a1*	1949.38288 ± 436.54152	1949.38288 ± 436.54152
a2*	-1326.44841 ± 420.14459	-1326.44841 ± 420.14459
a3*	418.14377 ± 130.48489	418.14377 ± 130.48489
a4*	-56.10286 ± 11.90528	-56.10286 ± 11.90528
a5*	5.09576 ± 1.19922	5.09576 ± 1.19922
b0*	19.35231 ± 0.43625	19.35231 ± 0.43625
b1*	-5.08947 ± 1.46464	-5.08947 ± 1.46464
b2*	3.14292 ± 1.35548	3.14292 ± 1.35548
b3*	-0.67493 ± 0.36335	-0.67493 ± 0.36335
T	298 ± 0	273 ± 0
Reduced Chi-Sqr*	7.61656E-4	
R□ □ (COD)	0.99955	0.99951
R□ □ (COD)*	0.99953	
□ □ □ R□ □ *	0.99946	

Figure S5. Virial fits for CO_2 on different temperature adsorption isotherms of MOF-801(Zr).

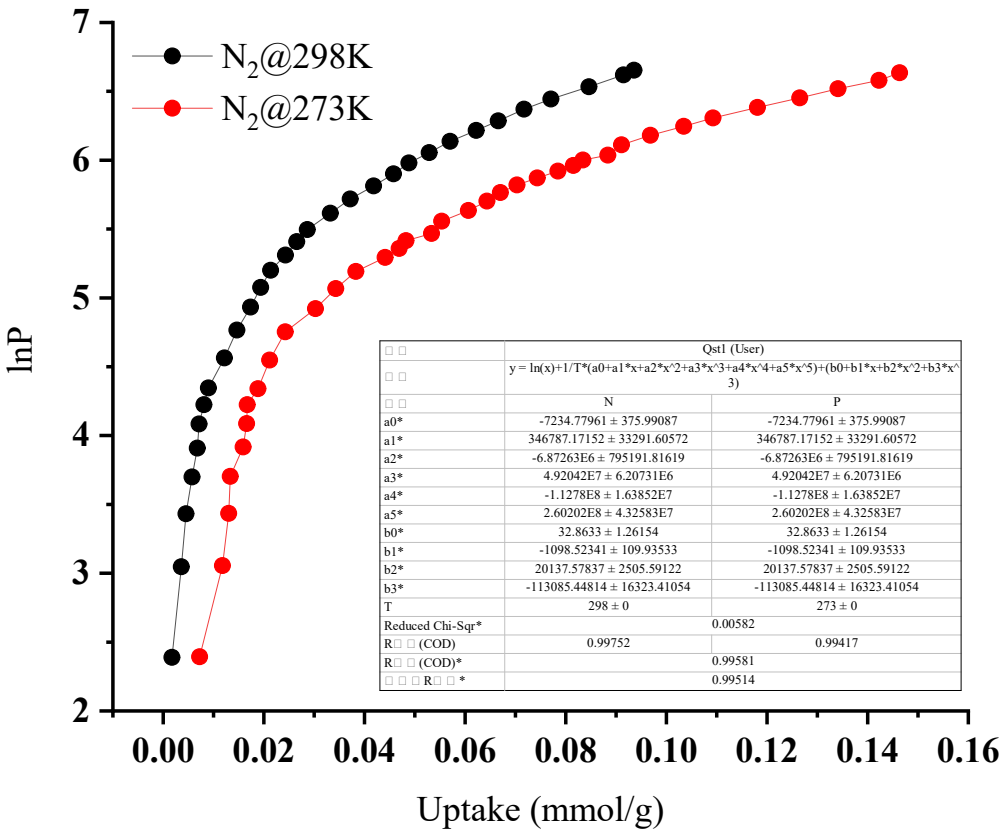

□ □	Qst1 (User)	
□ □	y = ln(x)+1/T*(a0+a1*x+a2*x^2+a3*x^3+a4*x^4+a5*x^5)+(b0+b1*x+b2*x^2+b3*x^3)	
□ □	N	P
a0*	-7234.77961 ± 375.99087	-7234.77961 ± 375.99087
a1*	346787.17152 ± 33291.60572	346787.17152 ± 33291.60572
a2*	-6.87263E6 ± 795191.81619	-6.87263E6 ± 795191.81619
a3*	4.92042E7 ± 6.20731E6	4.92042E7 ± 6.20731E6
a4*	-1.1278E8 ± 1.63852E7	-1.1278E8 ± 1.63852E7
a5*	2.60202E8 ± 4.32583E7	2.60202E8 ± 4.32583E7
b0*	32.8633 ± 1.26154	32.8633 ± 1.26154
b1*	-1098.52341 ± 109.93533	-1098.52341 ± 109.93533
b2*	20137.57837 ± 2505.59122	20137.57837 ± 2505.59122
b3*	-113085.44814 ± 16323.41054	-113085.44814 ± 16323.41054
T	298 ± 0	273 ± 0
Reduced Chi-Sqr*	0.00582	
R□ □ (COD)	0.99752	0.99417
R□ □ (COD)*	0.99581	
□ □ □ R□ □ *	0.99514	

Figure S6. Virial fits for N_2 on different temperature adsorption isotherms of MOF-801(Zr).

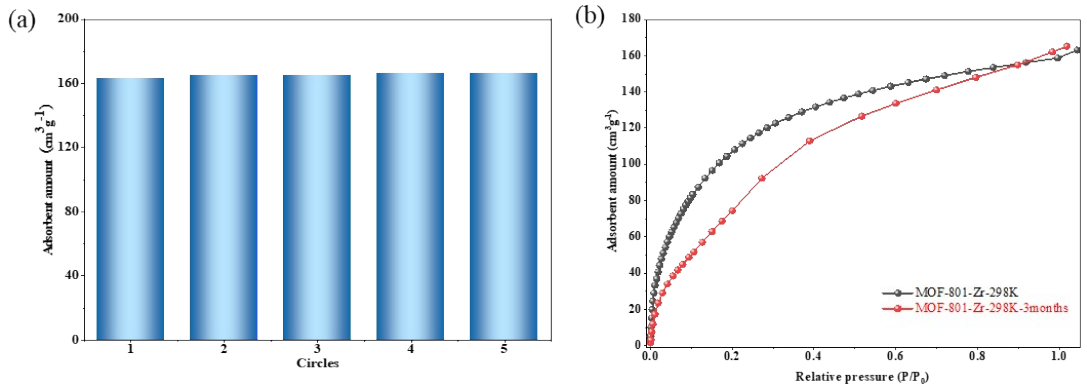

Figure S7. (a) The SO_2 adsorption performance in five-cycle testing (298 K). (b) Performance comparison of MOF-801(Zr) before and after three months of storage.

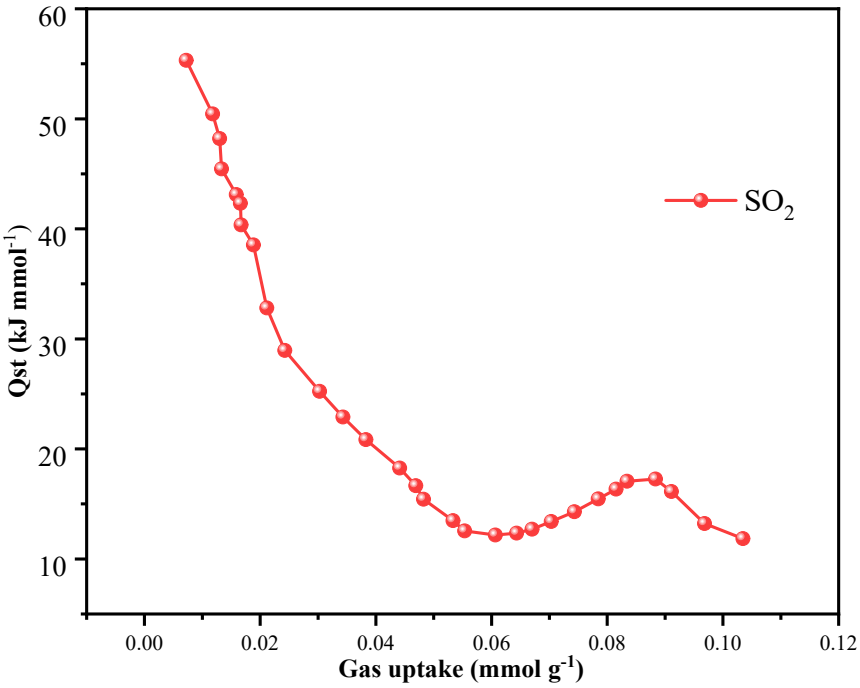

Figure S8. The Q_{st} of adsorption for N_2 for MOF-801(Zr).

For N_2, the Q_{st} value reported in the main text refers to the heat of adsorption at 1 bar. Given the linear nature and low uptake of the N_2 isotherms, the full Q_{st} curve for N_2 is omitted to maintain focus on the SO_2 capture performance.

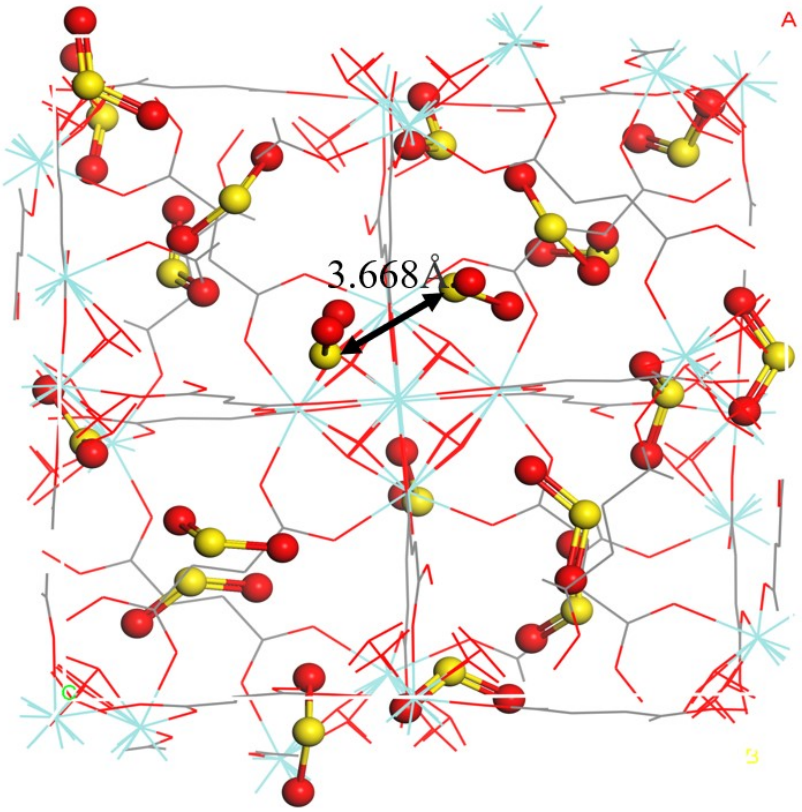

Figure S9. The GCMC simulation snapshots and the analysis of the intermolecular distances.

Table S1. Comparison of the uptake capacity of various adsorbents for SO_2 separation at 298 K.

Adsorbent	SO_2 uptake (mmol/g)	IAST Selectivity (SO_2/CO_2, 10/90)	IAST Selectivity (SO_2/N_2, 1/99)	Ref.
MOF-801(Zr)	7.28	35.8	86368	This work
MFM-300(In)	8.28	50	2700	[6]
NOTT-300	8.1	—	6522	[7]
Zr-bptc	7.8	600	18000	[8]
UIO-66-Cu	8.2	54	3100	[9]
SIFSIX-1-Cu	9.51	70.7	3145.7	[10]
Mg-gallate	7.61	321	$>1 \times 10^4$	[11]
HBU-23	4.57	58.9	2333.5	[12]
CPL-1	2.29	8.7	368	[13]
ZU-801	3.48	145	$>1 \times 10^4$	[14]
G808-N-10	15.7	83	2915	[15]
FJI-H14	9.91	47	6857 (10/90)	[16]
DMOF-ADC	6.51	75	—	[17]
NiNi-PYZ-NH_2	8.39	54.8(15/85)	—	[18]
DUT-67	9.3	37	20437	[19]
PCN-250(Fe_2Zn)	11.6	50	$>1 \times 10^4$	[20]
NanoCB_6-H	7.17	120	1720	[21]
ELM-12	3.3	30	871	[22]

Table S2. Crystallographic data and structure refinements for MOF-801(Zr).

MOF-801(Zr)	
Formula	$C_{24}H_{12}O_{32}Zr_6$
F.w.	1359.66
T (K)	363.15
Space group	*Pn-3*
a (Å)	17.8348(17)
b (Å)	17.8348(17)
c (Å)	17.8348(17)
α (°)	90
β (°)	90
γ (°)	90
V (Å^3)	5672.9(16)
Z	4
ρ_{calc}/mg mm^{-3}	1.592
m (mm^{-1})	1.450
R1 (>2σ/all date)	0.0619/0.1002
wR2 (>2σ/all date)	0.1553/0.1733
Largest diff. peak/hole / e Å^{-3}	1.45/-0.77

References

(1) Ju, Q.-Y.; Zheng, J.-J.; Xu, L.; Jiang, H.-Y.; Xue, Z.-Q.; Bai, L.; Guo, Y.-Y.; Yao, M.-S.; Zhu, T.-Y.*Nano Research,* **2023**, *17* (3), 2004-2010.

(2) Simon, C. M.; Smit, B.; Haranczyk, M. *Comput. Phys. Commun.,* **2016**, *200*, 364-38.

(3) Delley, B J. *Chem. Phys.,* **2000**, *113* (18), 7756-776.

(4) Casewit, C. J.; Colwell, K. S.; Rappe, A. K *J. Am. Chem. Soc.,* **1992**, *114* (25), 10035–10046.

(5) Metropolis, N.; Rosenbluth, A. W.; Rosenbluth, M. N.; Teller, A. H.; Teller, E J. *Chem. Phys.,* **1953**, *21* (6), 1087-1092.

(6) Savage, M.; Cheng, Y. G.; Easun, T. L.; Eyley, J. E.; Argent, S. P.; Warren, M. R.; Lewis, W.; Murray, C.; Tang, C. C.; Frogley, M. D.; Cinque, G.; Sun, J. L.; Rudic, S.; Murder, R. T.; Benham, M. J.; Fitch, A. N.; Blake, A. J.; Ramirez-Cuesta, A. J.; Yang, S. H.; Schröder, M.,*Advanced Materials* **2016,** *28* (39), 8705-8711.

(7) Yang, S. H.; Sun, J. L.; Ramirez-Cuesta, A. J.; Callear, S. K.; David, W. I. F.; Anderson, D. P.; Newby, R.; Blake, A. J.; Parker, J. E.; Tang, C. C.; Schröder, M., *Nature Chemistry* **2012,** *4* (11), 887-894.

(8) Li, J. N.; Smith, G. L.; Chen, Y. L.; Ma, Y. J.; Kippax-Jones, M.; Fan, M. T.; Lu, W. P.; Frogley, M. D.; Cinque, G.; Day, S. J.; Thompson, S. P.; Cheng, Y. Q.; Daemen, L. L.; Ramirez-Cuesta, A. J.; Schröder, M.; Yang, S. H., *Angewandte Chemie-International Edition* **2022,** *61* (36).

(9) Ma, Y. L.; Li, A. R.; Wang, C. *Chemical Engineering Journal* **2023,** *455*.

(10) Ji, Y.; Ma, T.; Yang, X. W.; Wang, R. S.; Wang, K.; Liu, X. Y.; Wang, X. L.; Jin, Q., *Journal of Hazardous Materials* **2025,** *496*.

(11) Chen, F. Q.; Lai, D.; Guo, L. D.; Wang, J.; Zhang, P. X.; Wu, K. Y.; Zhang, Z. G.; Yang, Q. W.; Yang, Y. W.; Chen, B. L.; Ren, Q. L.; Bao, Z. B. *Journal of the American Chemical Society* **2021,** *143* (24), 9040-9047.

(12) Gang, S. Q.; Liu, Z. Y.; Bian, Y. N.; Wang, R. H.; Du, J. L., *Separation and Purification Technology* **2024,** *335*.

(13) Zhang, Y.; Chen, Z. H.; Liu, X.; Dong, Z.; Zhang, P. X.; Wang, J.; Deng, Q.; Zeng, Z. L.; Zhang, S. H.; Deng, S. G. *Industrial & Engineering Chemistry Research* **2020,** *59* (2), 874-882.

(14) Yu, C.; Zhang, P. X.; Ding, Q.; Yang, L. F.; Suo, X.; Cui, X. L.; Xing, H. B., *Chemical Engineering Journal* **2023,** *471*.

(15) C. Zhou, C. Zheng, F. Liu, B. Yang, S. Zhang, H. Chen, S. Bai, C. Lin, C.-a. Tao and P. Ye, *Separation and Purification Technology*, 2025, **378**.

(16) S. Dou, P. Han, Z.-Z. Yang, J.-L. He, H. Zhang, Z.-D. Shao and L. Liang, *Chemical Engineering Journal*, 2026, **528**.

(17) S. Xing, A. Mohabbat, I. Boldog, J. Möllmer, M. Lange, Y. Haiduk, T. Heinen, V. Pankov, O. Weingart and C. Janiak, *Advanced Functional Materials*, 2025, DOI: 10.1002/adfm.202503013.

(18) Y. Li, Y. Sun, X. Bai, H. Song, W. Guo, S.-R. Zhao and Q. Chen, *Separation and Purification Technology*, 2025, **364**.

(19) X.-H. Xiong, Z.-W. Wei, W. Wang, L.-L. Meng and C.-Y. Su, *Journal of the American Chemical Society*, 2023, **145**, 14354-14364.

(20) J. Yao, Z. Zhao, L. Yu, J. Huang, S. Shen, S. Zhao, Y. Wu, X. Tian, J. Wang and Q. Xia, *Journal of Materials Chemistry A*, 2023, **11**, 14728-14737.

(21) J. Liang, S. Xing, P. Brandt, A. Nuhnen, C. Schlüsener, Y. Sun and C. Janiak, *Journal of Materials*

Chemistry A, 2020, **8**, 19799-19804.
(22) Y. Zhang, P. Zhang, W. Yu, J. Zhang, J. Huang, J. Wang, M. Xu, Q. Deng, Z. Zeng and S. Deng, *ACS Applied Materials & Interfaces*, 2019, **11**, 10680-10688.
(23) H. Furukawa, F. Gándara, Y.-B. Zhang, J. Jiang, W. L. Queen, M. R. Hudson and O. M. Yaghi, *Journal of the American Chemical Society*, 2014, **136**, 4369-4381